BIOCHEMISTRY
including biophysical chemistry & molecular biology
Article

Biochemistry **2010,** *49,* 5445–5454 5445
DOI: 10.1021/bi100639q

Structures and Binding Sites of Phenolic Herbicides in the Q_B Pocket of Photosystem II†

Ryouta Takahashi,§ Koji Hasegawa,‖ Akira Takano,§ and Takumi Noguchi*,§,‡

‡*Division of Material Science, Graduate School of Science, Nagoya University, Furo-cho, Chikusa-ku, Nogoya 464-8602, Japan,* §*Institute of Materials Science, University of Tsukuba, Tsukuba, Ibaraki 305-8573, Japan, and* ‖*AdvanceSoft Corporation, Akasaka, Tokyo 107-0052, Japan*

Received April 26, 2010; Revised Manuscript Received June 2, 2010

ABSTRACT: Herbicides targeting photosystem II (PSII) block the electron transfer beyond Q_A by binding to the Q_B site. Upon binding, the redox potential of Q_A shifts differently depending on the types of herbicides. In this study, we have investigated the structures, interactions, and locations of phenolic herbicides in the Q_B site to clarify the molecular mechanism of the Q_A potential shifts by herbicides. Fourier transform infrared (FTIR) difference spectra upon photoreduction of the preoxidized non-heme iron (Fe^{2+}/Fe^{3+} difference) were measured with PSII membranes in the presence of bromoxynil or ioxynil. The CN and CO stretching vibrations of these phenolic herbicides were identified at 2215−2200 and 1516−1505 cm^{-1}, respectively, in the Fe^{2+}/Fe^{3+} difference spectra. Comparison with the spectra of bromoxynil in ethanol solutions along with density functional theory analysis strongly suggests that the phenolic herbicides take a deprotonated form in the binding pocket. In addition, the CN stretching, NH bending, and NH stretching vibrations of a His side chain, which were found at 1109−1101, 1187−1185, and 3000−2500 cm^{-1}, respectively, in the Fe^{2+}/Fe^{3+} difference spectra, showed characteristic features in the presence of phenolic herbicides. These signals are probably attributed to D1-His215, one of the ligands to the non-heme iron. Docking calculations for herbicides to the Q_B pocket confirmed the binding of deprotonated bromoxynil to D1-His215 at the CO group, whereas the protonated form of bromoxynil and DCMU were found to bind to the opposite side of the pocket without an interaction with D1-His215. From these results, it is proposed that a strong hydrogen bond of the phenolate CO group with D1-His215 induces the change in the hydrogen bond strength of the Q_A CO group through the Q_A-His-Fe-His-phenolate bridge causing the downshift of the Q_A redox potential.

Photosystem II (PSII)[1] is a multisubunit complex that functions as water-quinone oxidoreductase in photosynthesis by plants and cyanobacteria. Upon light illumination, an electron is ejected from the excited state of Chl_{D1} to form a charge-separated state, $P680^+Pheo^-$ (*1*). On the electron donor side, $P680^+$ abstracts an electron from the Mn cluster, the catalytic site of water oxidation, through a redox-active tyrosine Y_Z (*2*). On the electron acceptor side, an electron is transferred from $Pheo^-$ to Q_A and then to Q_B (*3*). Upon two-electron reduction of Q_B, plastoquinone (PQ) in the Q_B pocket is converted to plastoquinol after binding two protons and is released from the pocket (*3*).

Herbicides targeting PSII are known to bind to the Q_B site and block the electron transfer beyond Q_A (*4*−*7*). Such herbicides can be categorized in several groups according to their chemical structures, that is, urea (e.g., DCMU), triazine (e.g., atrazine and terbutryn), uracil (e.g., bromacil), and phenolic (e.g., bromoxynil and ioxynil) type herbicides. In the studies of herbicide-resistant mutants, most types of herbicides lost sensitivity via mutations at D1-Ser264, one of the residues forming the Q_B pocket, whereas phenolic herbicides retain sensitivity, or rather show supersensitivity, to the Ser264 mutants (*4*−*6*). Thus, it has been suggested that the former and latter families of herbicides orient toward different amino acids in the binding pocket (*5*, *6*): the former to the D1-Ser264 side and the latter to the D1-His215 side. In these studies, the mutual positions of key amino acids were predicted from the X-ray structures of the bacterial reaction centers. Recently, the X-ray structures of PSII core complexes from cyanobacteria (*8*−*10*) revealed the locations of amino acid residues forming the Q_B pocket. However, orientations of herbicides in the Q_B pocket remain unknown because of the absence of X-ray structures of PSII in the presence of herbicides.

Binding of herbicides to PSII has been studied not only because of its function in blocking electron transfer but also because of the effect on the energetics of PSII relevant to photodamage and photoprotection (*11*, *12*). The redox potential of Q_A reduction is shifted differently depending on herbicide species bound to the Q_B site; phenolic herbicides lower the Q_A redox potential by ∼45 mV relative to that of control PSII without herbicides, whereas DCMU increases the potential by ∼50 mV (*13*). These potential changes are consistent with different peak temperatures of thermoluminescence by $S_2Q_A^-$ recombination between phenolic herbicides and other types of herbicides (*13*−*16*). The shifts of the Q_A redox potential affect the charge recombination pathways and their rates, which play

†This study was supported by the Grants-in-Aid for Scientific Research from the Ministry of Education, Culture, Sports, Science and Technology (21108506 and 21370063) to T.N. and a Grant-in-Aid for JSPS fellows (204647) to R.T.

*To whom correspondence should be addressed. Phone: +81-52-789-2881. Fax: +81-52-789-2883. E-mail: tnoguchi@bio.phys.nagoya-u.ac.jp.

[1]Abbreviations: DCMU, 3-(3,4-dichlorophenyl)-1,1-dimethylurea; DFT, density functional theory; FTIR, Fourier transform infrared; IR, infrared; Mes, 2-(*N*-morpholino)ethanesulfonic acid; P680, special pair chlorophylls in PSII; Pheo, redox-active pheophytin in PSII; PQ, plastoquinone; PSII, photosystem II; Q_A, primary quinone electron acceptor; Q_B, secondary quinone electron acceptor.

Published on Web 06/02/2010

significant roles in the photodamage and photoprotection of PSII (*11*, *12*). With a lower redox potential of Q_A, charge recombination via $P680^+Pheo^-$ is favored to form a triplet state that produces harmful singlet oxygen, whereas with a higher potential, a direct recombination pathway is dominant in safely relaxing the charged pair. For understanding the molecular mechanism of the Q_A potential shift by herbicide binding, it is essential to clarify the interactions of herbicides with specific amino acid residues in the Q_B pocket and how the interaction is transferred to Q_A.

We have recently investigated the effect of a herbicide on the hydrogen bond interaction of Q_A using Fourier transform infrared (FTIR) difference spectroscopy (*16*), a powerful method for studying the structures and interactions of redox cofactors and the coupled amino acid residues in photosynthetic proteins (*17*−*19*). It was found that phenolic herbicides downshift the CO frequency of the Q_A^- semiquinone radical, whereas other types of herbicides upshift the CO frequency, indicating that herbicide binding affects the hydrogen bond interaction of Q_A^- (*16*). Interestingly, the CN stretching band of a nitrile group in bromoxynil and ioxynil, typical phenolic herbicides, was detected in the Q_A^-/Q_A difference spectra of PSII membranes, providing evidence of an interaction between Q_A and phenolic herbicides. Because the CN frequency was closer to the phenolate form of bromoxynil than to its protonated form, it was suggested that phenolic herbicides are deprotonated in the Q_B pocket to interact with the imidazole of D1-His215 (*16*). Deprotonation of phenolic herbicides in the Q_B site was also suggested by Roberts et al. (*20*), taking into account the relatively low pK_a values of ~4.

In this study, we have further investigated the structures, interactions, and locations of phenolic herbicides in the Q_B pocket. For this purpose, we have measured the FTIR difference spectra of the non-heme iron upon its photoreduction (Fe^{2+}/Fe^{3+} difference) with PSII membranes in the presence of phenolic herbicides and compared them with the spectra without herbicides in the presence of DCMU. The interaction of herbicides with the non-heme iron should be stronger than that with Q_A, and hence, more information about herbicides and interacting amino acids is expected to be obtained. We have also performed docking calculations for herbicides to the Q_B pocket to identify the binding site in the pocket. The results provided evidence that phenolic herbicides take a deprotonated form strongly interacting with D1-His215 at the phenolate CO group. A mechanism of interaction transfer from a herbicide to Q_A to shift its redox potential is proposed.

MATERIALS AND METHODS

Sample Preparations. PSII-enriched membranes of spinach were prepared following the method previously described (*21*) and suspended in a pH 6.5 buffer containing 40 mM Mes, 400 mM sucrose, and 20 mM NaCl. Spinach in which nitrogen was globally labeled with ^{15}N was cultured as described previously (*22*). Mn depletion was performed by 10 mM NH_2OH treatment followed by several washes with the Mes buffer. The Mn-depleted PSII membranes were washed with a pH 8.0 buffer containing 100 mM Tris, 100 mM sucrose, 20 mM NaCl, and 50 mM sodium bicarbonate and finally suspended at a concentration of 0.5 mg of Chl/mL in the same buffer additionally containing 200 mM potassium ferricyanide and 0.1 mM herbicide (DCMU, bromoxynil, or ioxynil). The sample was then centrifuged at 170000*g* for 30 min, and the resulting pellet was sandwiched between two CaF_2 plates (25 mm in diameter). One of the CaF_2 plates has a circular groove (14 mm inner diameter, 1 mm width), and the sample cell was sealed with silicone grease laid on the outer part of the groove, where a piece of aluminum foil (~1 mm × 1 mm; ~15 μm thick) was placed as a spacer (*23*). The sample temperature was adjusted to 10 °C by circulating cold water in a copper holder. The sample was stabilized at this temperature in the dark for more than 1 h before measurements were taken.

FTIR Measurements. Flash-induced FTIR spectra were recorded on a Bruker IFS-66/S spectrophotometer equipped with an MCT detector (D313-L) at 4 cm^{-1} resolution. Flash illumination was performed using a Q-switched Nd:YAG laser (INDI-40-10, 532 nm, ~7 ns full width at half-maximum, 10 mJ $pulse^{-1}$ cm^{-2}). Single-beam spectra with 50 scans (accumulation for 25 s) were recorded before and after single-flash illumination. The measurement was repeated with an interval of 300 s for dark relaxation. The spectra obtained by more than 300 cycles using a couple of samples were averaged to calculate a Fe^{2+}/Fe^{3+} difference spectrum by subtraction of the spectrum before illumination from that after illumination. FTIR spectra of bromoxynil and its deprotonated form in ethanol (50 mM) were recorded at room temperature using an attenuated total reflection (ATR) accessory (DuraSamp1*IR*II, Smiths Detection) with a three-reflection silicon prism (3 mm diameter) (*16*). The deprotonated form of bromoxynil was prepared by addition of a 3% volume of a 2.5 M NaOH/water solution to a bromoxynil ethanol solution. FTIR spectra of solvents were subtracted from those of sample solutions to eliminate the contributions of solvents.

DFT Calculations. Molecular orbital calculations were performed using the Gaussian03 program package (*24*). The B3LYP functional (*25*, *26*) with the 6-31+G(d) basis set was used to optimize the geometries of model complexes and calculate their vibrational frequencies and IR intensities. When the vibrations of a water molecule as a hydrogen bond partner in the complexes of bromoxynil were strongly coupled with its CO vibration, such coupling was removed by substitution of hydrogen with a deuteron in the water molecule.

Docking Calculation. The initial atomic coordinates of the D1 and D2 proteins were taken from the X-ray structure of the PSII complexes from *Thermosynechococcus elongatus* at 2.9 Å resolution [Protein Data Bank (PDB) entry 3BZ1 (*9*)]. The hydrogen atoms were added with Reduce (*27*) assuming physiological pH. To structurally refine the Q_B binding pocket, we performed partial geometry optimization for the Q_B site, including the non-heme iron, its four histidine ligands (D1-His215, D1-His272, D2-His214, and D2-His268), and the D1 residues around a plastoquinone ring of Q_B (Met214, Leu218, Val219, Tyr246, Ile248, Ala251, His252, Phe255, Ser264, Phe265, and Leu271). The geometry optimization was conducted by molecular mechanics calculation with the combination of the universal force field method (*28*) and the modified charge equilibration (MQEq) method (*29*) in the ABINIT-MP program package (*30*, *31*). In the MQEq method, atomic charge parameters of Rappé and Goddard (*32*) were used. All docking calculations were performed with AutoDock (*33*, *34*). The molecular structures of herbicides and PQ-1 were optimized using molecular mechanics calculations with the AMBER force field (*24*). The docking pocket was set to a 20 Å cube with a 0.2 Å grid spacing centered at the Q_B ring. The MQEq atomic charges of the protein and the herbicides were used to calculate the electrostatic potential maps in the pocket and an empirical binding free energy (*35*) during the docking calculation. The Lamarckian genetic algorithm (*35*) was

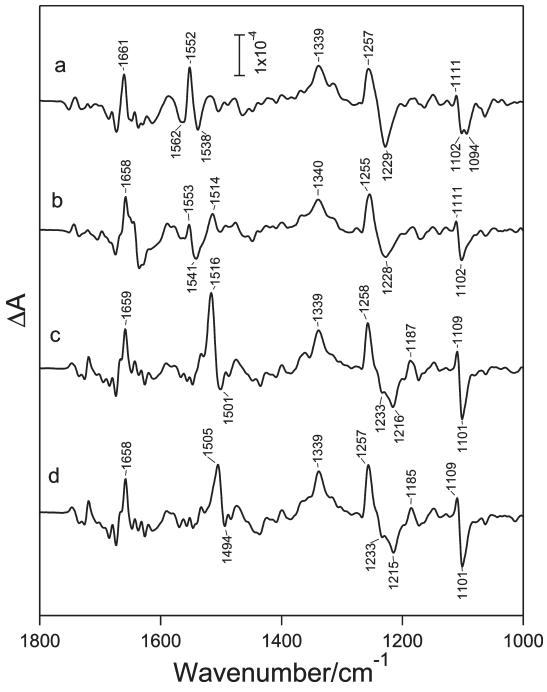

FIGURE 1: Light-induced Fe^{2+}/Fe^{3+} FTIR difference spectra (1800−1000 cm^{-1} region) of PSII membranes in the absence of herbicides (a) and in the presence of DCMU (b), bromoxynil (c), and ioxynil (d).

utilized to search the conformation of the PQ-1 and herbicides in the pocket.

RESULTS

Fe^{2+}/Fe^{3+} FTIR Difference Spectra. Figure 1a shows a flash-induced FTIR difference spectrum in the 1800−1000 cm^{-1} region of the non-heme iron in the control Mn-depleted PSII membranes in the absence of herbicides at pH 8.0. The non-heme iron was preoxidized to Fe^{3+} by ferricyanide and reduced to Fe^{2+} upon single-flash illumination, and thus, the spectrum represents the Fe^{2+}/Fe^{3+} difference involving the information of the structural changes in proteins and cofactors coupled to the iron center. Positive and negative peaks at 2116 and 2039 cm^{-1}, respectively, arising from the CN stretches of ferricyanide and ferrocyanide were observed (data not shown), indicating that ferrocyanide works as an electron donor in this reaction. This spectrum was virtually identical to the previous Fe^{2+}/Fe^{3+} spectra measured using PSII membranes of spinach (*36*−*38*) and cyanobacterial PSII core complexes (*39*, *40*). The peaks in the 1700−1600 and 1600−1500 cm^{-1} mainly arise from the amide I (the C=O stretch of backbone amides) and amide II (the NH bend coupled with the CN stretch of backbone amides) vibrations indicative of perturbations of polypeptide chains upon Fe reduction (*36*). The positive and negative bands at 1339 and 1229 cm^{-1}, respectively, were assigned to the CO stretches of bicarbonate, a ligand of the non-heme iron, by introduction of [^{13}C]bicarbonate (*36*), while the positive peak at 1257 cm^{-1} and the part of the 1229 cm^{-1} negative band were attributed to the CO stretching vibration of a Tyr side chain (either D1-Tyr246 or D2-Tyr244) structurally coupled to the iron center by [4-^{13}C]Tyr labeling (*40*). The peaks at 1111(+), 1102(−), and 1094(−) cm^{-1} are due to the CN stretching vibrations of the imidazole ring of the His ligands (*36*, *38*). The 8 cm^{-1} lower frequency of the 1094 cm^{-1} peak compared to that of the 1102 cm^{-1} peak has been attributed to deprotonation of one of the four His ligands, most probably D1-His215, to become an imidazolate form in the Fe^{3+} state (*36*, *38*). Such a downshift of the His CN mode upon imidazolate formation has been observed in FTIR measurements of histidine and its model complex, 4-methylimidazole (*48*, *49*), and reproduced by DFT calculations (*49*).

Fe^{2+}/Fe^{3+} difference spectra of PSII membranes in the presence of herbicides are presented in Figure 1b−d. In the presence of DCMU, the intensity of the 1552 cm^{-1} peak in the amide II region significantly decreased and that of the 1094 cm^{-1} peak of the imidazolate form also became smaller to give a shoulder of the 1102 cm^{-1} band. In addition, the strong positive peak at 1661 cm^{-1} in the amide I region slightly downshifted by 3 cm^{-1}. The bicarbonate peaks were observed at 1340 and 1228 cm^{-1}, which agreed with the frequencies of the corresponding peaks in the control spectrum within 1 cm^{-1}. The spectra of PSII in the presence of bromoxynil (Figure 1c) and ioxynil (Figure 1d) exhibited very similar features. When compared with the control spectrum, the amide I peak is found at lower frequencies by 2−3 cm^{-1} and the feature of the negative band at 1229 cm^{-1} due to the bicarbonate CO group is changed to a peak at 1216−1215 cm^{-1} with a shoulder at 1233 cm^{-1}, whereas the positive band at 1339 cm^{-1} arising from the bicarbonate CO group in the Fe^{2+} state was unchanged. The His peaks at 1111(+) and 1102(−) cm^{-1} slightly downshift to 1109(+) and 1101(−) cm^{-1}, respectively, with increased intensities, and the negative peak at 1094 cm^{-1} disappeared. Such shifts of the 1111 and 1102 cm^{-1} peaks were not observed in the case of DCMU binding (Figure 1b). Another characteristic of the spectra with bromoxynil and ioxynil is the appearance of a strong positive peak at 1516 and 1505 cm^{-1}, respectively. The frequency difference of 11 cm^{-1} for these peaks is actually the only difference between the two spectra appreciable in the 1800−1000 cm^{-1} region.

The spectral region around these positive peaks is expanded in Figure 2A (solid line, bromoxynil; dotted line, ioxynil). The frequency gap of the two prominent peaks without notable changes in other bands is clearly shown. The peaks at 1516 and 1505 cm^{-1} were virtually unaffected by the measurements in D_2O buffer (data not shown), excluding the contribution from the amide II vibrations of polypeptide chains in hydrophilic domains around the Q_B site. Also, if these peaks were attributed to the amide II vibrations, drastic changes only in the amide II bands without large changes in the amide I region would be unreasonable. Thus, it is most likely that these peaks are attributed to bromoxynil and ioxynil themselves that are coupled to the non-heme iron reaction, and the frequency gap originates from the slight structural difference between these herbicides. The structural coupling of bromoxynil and ioxynil with the non-heme iron is also exhibited by the appearance of the CN stretching bands of their nitrile groups (see below).

Figure 2B shows the same region of the FTIR spectra of bromoxynil (thin line) and its deprotonated phenolate form (thick line) dissolved in ethanol. The most prominent feature in this region is strong bands at 1476 and 1485 cm^{-1} for protonated and deprotonated bromoxynil, respectively, due to the CO stretching vibrations (see below for assignments). Thus, the peaks at 1516 and 1505 cm^{-1} in the Fe^{2+}/Fe^{3+} spectra (Figure 2A) are likely to be attributed to the CO stretching vibrations of bromoxynil and ioxynil, respectively, bound to the Q_B site in either the protonated or the deprotonated form. Weak negative bands at 1501 and 1494 cm^{-1} (Figure 2A), in the presence of bromoxynil and ioxynil, respectively, on the lower-frequency sides of the major positive bands may be due to the corresponding CO bands in the Fe^{3+} state.

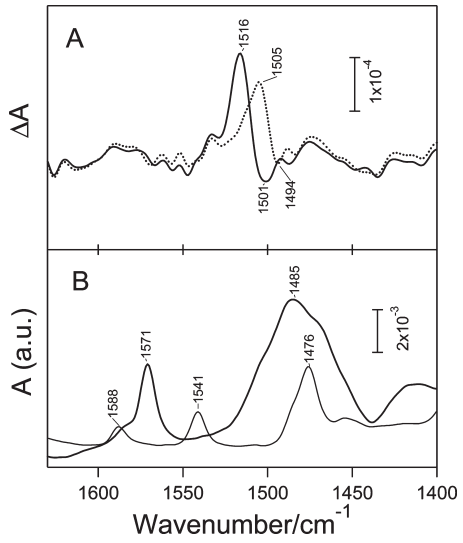

FIGURE 2: (A) CO stretching region of bromoxynil (solid line) and ioxynil (dotted) in the Fe^{2+}/Fe^{3+} FTIR difference spectra. (B) CO stretching region of the FTIR spectra of bromoxynil in the protonated (thick line) and deprotonated (thin line) forms dissolved in ethanol. Solvent bands were subtracted from the solution spectra.

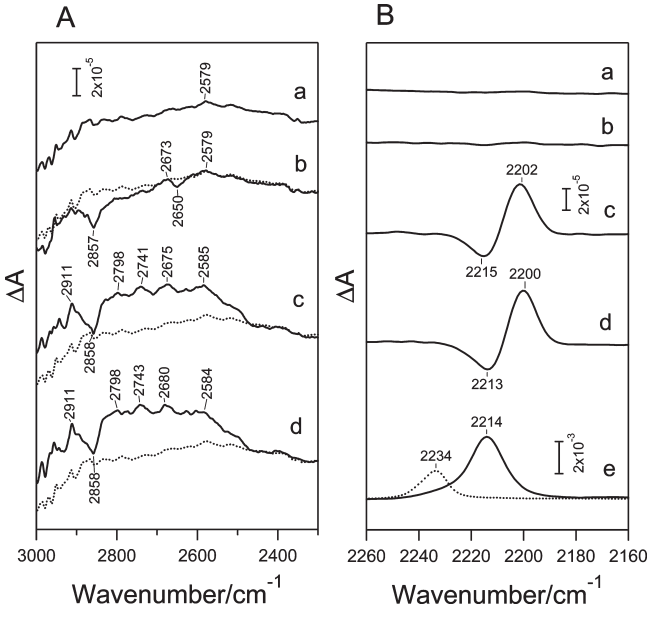

FIGURE 3: Fe^{2+}/Fe^{3+} FTIR difference spectra of PSII membranes. (A) 3000−2300 cm^{-1} region (His NH region) in the absence of herbicides (a) and in the presence of DCMU (b, solid line), bromoxynil, (c, solid line), and ioxynil (d, solid line). In parts b−d, the spectrum in the absence of herbicides (the spectrum in part a) is shown for comparison (dotted lines). (B) 2260−2160 cm^{-1} region (CN stretching region) in the absence of herbicides (a) and in the presence of DCMU (b), bromoxynil (c), and ioxynil (d), in comparison with the FTIR spectra of bromoxynil (e) in protonated (solid line) and deprotonated (dotted line) forms dissolved in ethanol.

Figure 3A shows the Fe^{2+}/Fe^{3+} difference spectra in the higher-frequency region of 3000−2300 cm^{-1}, where broad continuum bands arising from polarized protons in strong hydrogen bonds appear (*41*). Previous FTIR difference spectra upon Q_A and Q_B photoreduction (*42*−*45*) and the $S_1 \rightarrow S_2$ transition of the oxygen-evolving center (*46*) have shown that several small peaks on a broad feature in this region originate from the Fermi resonance of a His NH vibration coupled with the overtones and combinations of other fundamental His vibrations, indicative of the presence of a strongly hydrogen-bonded imidazole group coupled to the cofactor. The samples in the absence of herbicides (Figure 3Aa) showed only some weak peaks centered at 2579 cm^{-1} on a weak continuum band. In the presence of DCMU (Figure 3Ab, solid line), additional features appeared at 2857, 2673, and 2650 cm^{-1}, although the overall intensity of a broad background did not change. In sharp contrast, in the presence of bromoxynil (Figure 3Ac, solid line) and ioxynil (Figure 3Ad, solid line), a broad background became significantly intense above 2500 cm^{-1} and several prominent peaks (e.g., 2911, 2858, 2798, 2741−2743, 2675−2680, and 2584−2585 cm^{-1}) were observed on this background. Indeed, this large broad band in the high-frequency region is a characteristic of phenolic herbicides; other types of herbicides, not only DCMU (urea type) but also bromacil (uracil type) and atrazine (triazine type), exhibited features similar to those of the control sample (data not shown). In addition, Berthomieu and Hienerwadel previously showed that the broad continuum band was totally absent in the presence of *o*-phenanthroline (*38*).

Bromoxynil and ioxynil have a nitrile group in the phenolic ring (see the structure of bromoxynil in Figure 6) and hence are expected to show a CN stretching band in the 2260−2200 cm^{-1} region (*47*), if they are coupled to the iron center. We previously observed the CN stretching bands of bromoxynil and ioxynil at 2205/2216 and 2203/2213 cm^{-1}, respectively, in the Q_A^-/Q_A difference spectra of PSII membranes in the presence of these herbicides (*16*). Similar peaks were observed at 2202/2115 and 2200/2213 cm^{-1} in the Fe^{2+}/Fe^{3+} difference spectra with bromoxynil (Figure 3Bc) and ioxynil (Figure 3Bd), respectively, whereas no band was observed in this region in the absence of herbicides (Figure 3Ba) and in the presence of DCMU (Figure 3Bb). The CN bands of bromoxynil and its deprotonated phenolate form in ethanol, which we previously reported (*16*), are presented in Figure 3Be (dotted and solid lines, respectively). The protonated bromoxynil had a CN peak at 2234 cm^{-1}, while the deprotonated form showed a peak at 2214 cm^{-1}, a frequency lower by 20 cm^{-1}, with an intensity ~2 times higher.

To confirm the assignments of His vibrations in the Fe^{2+}/Fe^{3+} spectrum, the spectrum of globally ^{15}N-labeled PSII membranes in the presence of bromoxynil was obtained (Figure 4Aa,B, red lines) and compared with the spectra of the unlabled sample (Figure 4Aa,B, black lines). In the 1800−1000 cm^{-1} region (Figure 4A), appreciable changes are observed in the bands around 1100 cm^{-1} as expected and the peaks at 1109 and 1101 cm^{-1} downshifted by 7 cm^{-1} to 1102 and 1194 cm^{-1}, respectively. Another change was observed as a downshift of a small peak from 1187 to 1180 cm^{-1} (by 7 cm^{-1}). The double difference spectrum (Figure 4Ab) more clearly showed these changes. The prominent signal at 1110/1101/1089 cm^{-1} and the small signal at 1189/1178 cm^{-1} correspond to the frequency changes mentioned above. Numerous peaks in the 1700−1600 and 1600−1500 cm^{-1} regions are most likely due to the amide I and amide II vibrations, respectively, although higher noise levels in these regions and the fact that these bands are sensitive to subtle changes in sample conditions hamper definite identification of isotope effects. It is now safe to say that the peaks at 1109/1101 cm^{-1} in the presence of bromoxynil arise from the His CN vibrations, which have shown bands around 1100 cm^{-1} in the FTIR spectra of histidine and 4-methylimidazole, a model compound of a His side chain, and in DFT calculations (*46*, *48*−*50*). The 1187 cm^{-1} band is most likely attributed to the NH bending band of imidazole, which was observed at 1151 cm^{-1} in 4-methylimidazole in aqueous

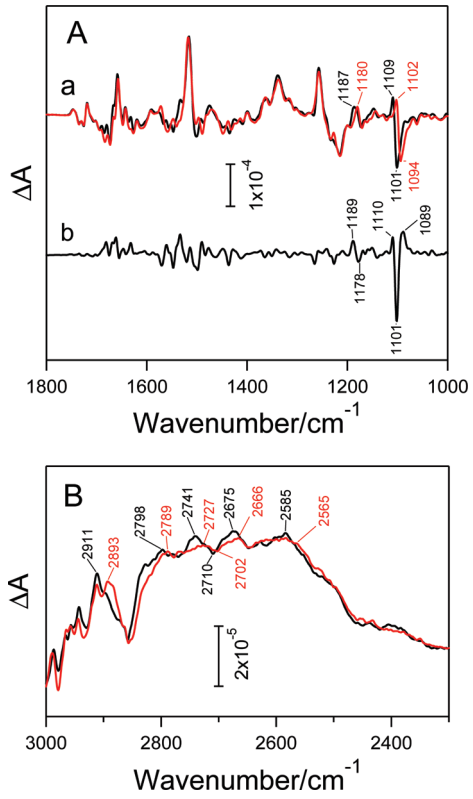

FIGURE 4: (A) (a) Fe^{2+}/Fe^{3+} FTIR difference spectrum (1800−1000 cm^{-1} region) of globally ^{15}N-labeled PSII membranes in the presence of bromoxynil (red line) in comparison with that of unlabeled PSII membranes (black line). (b) Unlabeled-minus-^{15}N-labeled double difference spectrum. (B) 3000−2300 cm^{-1} region of the Fe^{2+}/Fe^{3+} FTIR difference spectrum of globally ^{15}N-labeled PSII membranes in the presence of bromoxynil (red line) in comparison with that of unlabeled PSII membranes (black line).

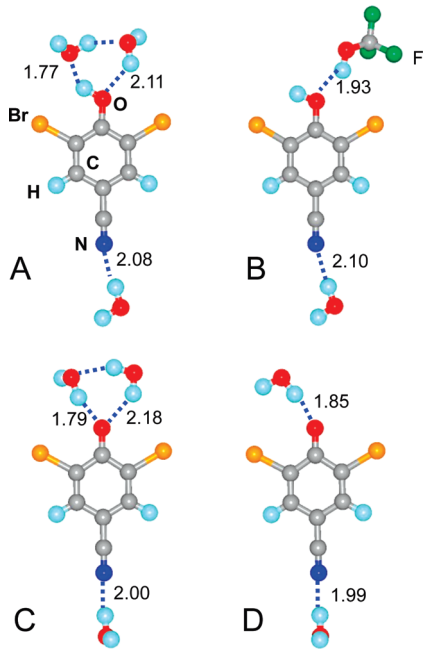

FIGURE 5: Optimized geometries of the hydrogen-bonded complexes of bromoxynil in the protonated (A and B) and deprotonated phenolate (C and D) forms obtained by DFT calculations at the B3LYP/6-31+G(d) level. In all models, the nitrogen atom of the CN group is hydrogen bonded with a H_2O molecule. The OH group of bromoxynil is hydrogen bonded with two H_2O molecules (A) or CF_3OH (B), and the phenolate oxygen of the deprotonated bromoxynil is hydrogen bonded with two H_2O molecules (C) or one (D).

solution (*43*). Note that a similar peak was observed at 1185 cm^{-1} in the spectrum with ioxynil (Figure 1d), whereas no corresponding band was clearly observed in the control spectrum (Figure 1a) and the spectrum with DCMU (Figure 1b). Several peaks at 3000−2500 cm^{-1} on a broad background also showed downshifts of 8−20 cm^{-1} upon ^{15}N labeling, providing evidence that these features are due to the Fermi resonance peaks of a His side chain.

DFT Calculations of Hydrogen-Bonded Complexes of Bromoxynil. To understand the effects of deprotonation of the phenolic OH group of bromoxynil and its hydrogen bond interactions on the CN and CO stretching frequencies, we performed DFT calculations for the model complexes of bromoxynil in the protonated (Figure 5, models A and B) and deprotonated (Figure 5, models C and D) forms. Figure 5 shows the optimized geometries of these models. In models A and C, the phenolic OH group or the phenolate oxygen and the CN group are fully hydrogen bonded with three H_2O molecules (the OH group or phenolate oxygen has two hydrogen bonds, and the CN group has one hydrogen bond), while models B and D have one hydrogen bond at the oxygen atom with CF_3OH and H_2O, respectively, keeping a hydrogen bond at the CN group. The reason for using CF_3OH, a stronger hydrogen bond donor than H_2O, in model B is that the basicity of the oxygen of the phenolic OH group was not high enough to form a stable hydrogen-bonded complex with H_2O. The obtained CN and CO stretching frequencies and their infrared intensities are summarized in Table 1 together with experimental results from Figures 2 and 3. Note that calculated CN and CO frequencies were scaled with different scaling factors of 0.9657 and 0.9378, respectively, to adjust the frequencies of model B (a phenolate form with full hydrogen bonding) to the experimental data of deprotonated bromoxynil in ethanol. This scaling was performed to facilitate comparison between calculated and experimental results, and thus, frequency differences between the models rather than the absolute values are important in this analysis.

When CN stretching frequencies of fully hydrogen-bonded bromoxynil (model A) and its deprotonated form (model C) were compared, the latter showed a lower frequency by 40 cm^{-1} and a stronger intensity by a factor of 4.7. This is consistent with the experimental data in ethanol which showed that the phenolate form exhibited a lower CN frequency by 20 cm^{-1} with a 2 times larger intensity compared with that of the protonated bromoxynil (Figure 3Be and Table 1), although the frequency gap was estimated to be much larger via calculation. When one of the two hydrogen-bonded H_2O molecules at the CO group of the deprotonated bromoxynil in model C was removed (model D), the CN frequency downshifted by 6 cm^{-1}. On the other hand, when the hydrogen bond to the OH group hydrogen was removed from model A and the OH group oxygen was engaged in a hydrogen bond with CF_3OH (model B), the CN frequency upshifted by 5 cm^{-1}.

The CO stretching vibration of model C of deprotonated bromoxynil (1485 cm^{-1}) showed a frequency higher than that of model A of protonated bromoxynil (1421 cm^{-1}) by 64 cm^{-1} and a stronger intensity by a factor of ~3 (Table 1). The tendency to upshift is similar to the experimental result in ethanol solutions, although the extent of the upshift was much smaller (9 cm^{-1}) in experiments. When the double hydrogen bonds at the phenolate oxygen (model C) are reduced to a single hydrogen bond (model D), the CO frequency further upshifted by 38 cm^{-1}. In contrast,

Table 1: Calculated and Experimental Frequencies (cm^{-1}) of the CN and CO Stretching Vibrations of Bromoxynil

protonation state	condition	CN stretch[b] (int)[c]	CO stretch[b] (int)[c]
	Calculated[a]		
protonated	with $3H_2O$ (model A)	2263 (123)	1421 (190)
	with $2H_2O$ and CF_3COOH (model B)	2268 (83)	1412 (202)
deprotonated	with $3H_2O$ (model C)	2213 (582)	1485 (582)
	with $2H_2O$ (model D)	2207 (624)	1523 (598)
	Experimental		
protonated	in EtOH	2234	1476
deprotonated	in EtOH	2214	1485
	in PSII (Fe^{2+}, neutral Q_A)	~2209[d]	1516

[a]Vibrational frequencies were calculated using the DFT method at the B3LYP/6-31+G(d) level. [b]Calculated frequencies were scaled with scaling factors of 0.9657 and 0.9378 for the CN and CO vibrations, respectively, to adjust the calculated values of model C to the experimental values of the phenolate anion form in EtOH. [c]Infrared intensities in parentheses were calculated in kilometers per mole. [d]The CN frequency of bromoxynil was estimated from the data of the Fe^{2+}/Fe^{3+} difference spectrum in this study and the Q_A^-/Q_A difference spectrum in ref *16* (see the text for details).

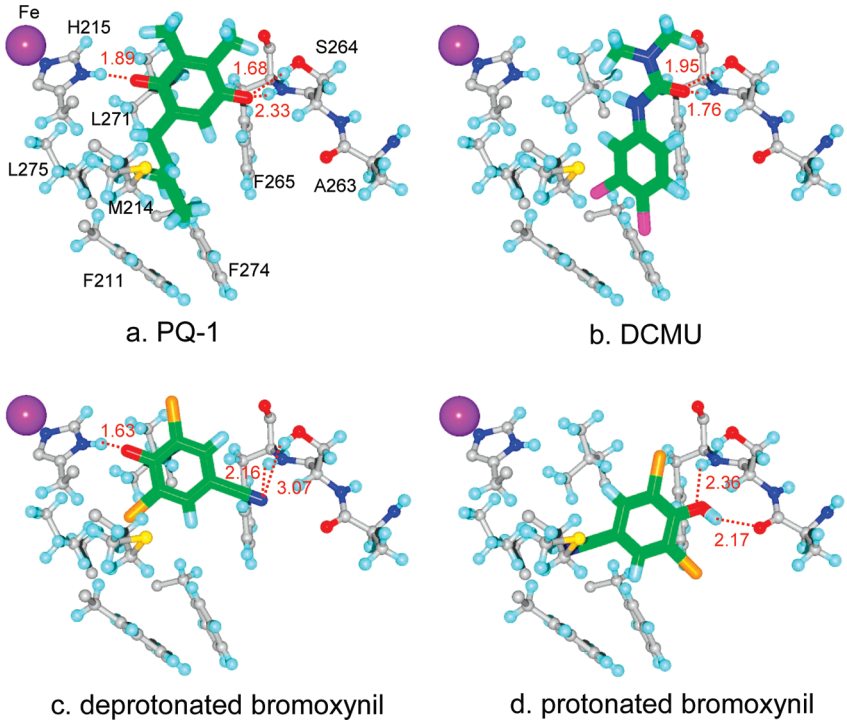

FIGURE 6: Binding sites of PQ and herbicides in the Q_B pocket of PSII obtained by docking calculations: (a) PQ-1, (b) DCMU, (c) deprotonated bromoxynil, and (d) protonated bromoxynil. All amino acid residues labeled in panel a belong to the D1 subunit. D1-L218 and D1-F255 that are also residues in the Q_B pocket and located on the upper side of the plane have been omitted so that the interactions of PQ-1 and herbicides are clearly shown. The Q_B binding site was once optimized using the X-ray structure by Guskov et al. [2.9 Å resolution (*9*)] by a molecular mechanics calculation, and then docking calculations of PQ-1 and herbicides were performed for the optimized Q_B pocket.

when the OH group of protonated bromoxynil has a single hydrogen bond as a hydrogen bond acceptor (model B), the CO frequency was lower by 9 cm^{-1} than that of model A in which the OH group both donates and accepts a hydrogen bond with two H_2O molecules.

Docking Calculation for Herbicides in the Q_B Pocket. To model the binding site of herbicides in the Q_B pocket, docking calculations were performed for PQ-1, DCMU, bromoxynil, and its deprotonated phenolate form. Proper docking of a PQ model to the Q_B site was not successful when the protein structure determined via X-ray crystallography at 2.9 Å resolution by Guskov et al. (*9*) was directly used. This is probably because the structure of the Q_B pocket is not sufficiently accurate in the X-ray structure because of the limited resolution. Hence, we performed structural optimization of the Q_B site, including the non-heme iron, Q_B, and surrounding amino acids using molecular mechanics calculations. When the docking calculation of PQ-1 as a Q_B model was performed for the optimized Q_B pocket, proper PQ binding very similar to the Q_B position in the X-ray structure was reproduced (Figure 6a), indicating the reliability of the docking calculation. The central part of the Q_B pocket is formed with hydrophobic Phe and Leu residues, i.e., Phe255, Phe265, Phe274, Phe211, Leu218, Leu271, and Leu275 (Leu218 and Phe255 have been omitted from Figure 6 so that the interactions of PQ-1 and herbicides are clearly shown), while polar groups are located at both ends of the pocket: the imidazole of D1-His215 at one end and the OH group of D1-Ser264, the backbone NH group of D1-Phe265, and the backbone C=O group of D1-Ala263 at the other

end (Figure 6). In this pocket, one of the C=O groups of PQ-1 is hydrogen bonded to His215 and the other C=O group interacts with Ser264 and the backbone NH group of Phe265 (Figure 6a).

Docking calculations for DCMU resulted in the binding to the pocket interacting with the Ser264 OH and Phe265 NH groups through the C=O group in a trans-amide conformation without an interaction with His215 (Figure 6b). This is consistent with the previous observations of DCMU tolerance induced by Ser264 mutations (*5*, *6*). In contrast, our docking result is at odds with the previously calculated binding models, in which DCMU is hydrogen bonded with His215 at the C=O group in a trans-amide conformation (*51*, *52*) or with the OH group oxygen of Ser264 at the phenylamino NH group in a cis-amide conformation (*51*). However, these previous modeling studies were performed before the report of the X-ray structure of PSII core complexes and thus based on the D1 model predicted from the X-ray structure of the bacterial reaction center.

When the phenolate form of bromoxynil was applied to the docking calculation, it resulted in a strong interaction with His215 through a hydrogen bond between the phenolic CO group and the imidazole NH group (Figure 6c). The nitrogen of the CN group interacts with the Phe265 NH group (the N···H distance is 2.16 Å), whereas the interaction with the Ser264 OH group seems to be much weaker (the N···H distance is 3.07 Å). On the other hand, protonated bromoxynil did not interact with His215 at all but interacted with the backbone C=O group of Ala263 and the NH group of Phe265 through the hydrogen and oxygen atoms, respectively, of the phenolic OH group (Figure 6d). This binding site is in contrast to the previous modeling of neutral ioxynil, in which ioxynil is located in the pocket in an orientation similar to that in our model of deprotonated bromoxynil, i.e., an interaction with H215 and Ser264/Phe265 (*52*). This discrepancy may originate not only from the usage of the D1 model deduced from the bacterial reaction center but also from their modeling method, in which only the contact surface between atoms was taken into account without estimation of interaction energy, whereas our docking calculation includes estimation of the electrostatic, van der Waals, and hydrogen bonding interactions. Thus, the weak basicity of the oxygen of the phenolic OH group as a hydrogen bond acceptor in comparison with the strong basicity of the phenolate oxygen was not reflected in the previous model.

DISCUSSION

In this study, we have determined the protonation structure, hydrogen bond interactions, and binding sites of phenolic herbicides in the Q_B pocket of PSII using FTIR difference spectroscopy and docking calculations. Fe^{2+}/Fe^{3+} FTIR difference spectra provided the structural information about the herbicide bound to the Q_B site as well as the protein moieties around the non-heme iron. Docking calculations for herbicides to the Q_B pocket supported the FTIR results and directly visualized the binding sites and the orientations of herbicides in the pocket.

Protonation Structure of Bromoxynil and Ioxynil. The CN stretching bands of bromoxynil and ioxynil were detected as differential signals at 2202/2215 and 2200/2213 cm^{-1}, respectively, in the Fe^{2+}/Fe^{3+} FTIR difference spectra. This indicates that these herbicides are structurally coupled to the non-heme iron center and their molecular interactions are affected by the redox change of the iron. The observed frequencies are similar to those in the previously reported Q_A^-/Q_A difference spectra, 2205/2216 and 2203/2213 cm^{-1} for bromoxynil and ioxynil, respectively (*16*). In the Q_A^-/Q_A FTIR measurements, the non-heme iron remained in the Fe^{2+} state due to the presence of NH_2OH. The discrepancies of the peak frequencies for the same PSII state with neutral Q_A and Fe^{2+} between the Fe^{2+}/Fe^{3+} and Q_A^-/Q_A difference spectra, i.e., 2202 cm^{-1} versus 2216 cm^{-1} for bromoxynil and 2200 cm^{-1} versus 2213 cm^{-1} for ioxynil, indicate that the real CN frequencies are located near the centers of the two peaks, at ~2209 and ~2207 cm^{-1} for bromoxynil and ioxynil, respectively, and slight shifts upon redox changes of Fe and Q_A induce the differential signals.

As already discussed in our previous report of the CN peaks in the Q_A^-/Q_A difference spectra (*16*), these CN frequencies are closer to the frequency of the phenolate form of bromoxynil in ethanol, 2214 cm^{-1}, rather than that of the protonated form, 2234 cm^{-1} (Figure 3Be), suggesting that bromoxynil is deprotonated in the Q_B pocket. The decrease in the CN frequency of bromoxynil by deprotonation concomitant with an intensity increase (Figure 3Be) was also reproduced by DFT calculations (Figure 5 and Table 1).

The CO stretching vibrations of bromoxynil in the protonated and deprotonated forms were observed at 1476 and 1485 cm^{-1}, respectively, in ethanol solutions (Figure 2B). The DFT calculations of model hydrogen-bonded complexes of bromoxynil supported this assignment (Table 1). These CO frequencies that are significantly higher than the CO frequency region of *p*-cresol [1280−1220 cm^{-1} (*53*)] are attributed to the shorter C−O bond length due to the strong electron withdrawing abilities of the Br groups at the ortho positions and of the CN group at the para position of the phenyl ring. Indeed, our DFT calculations at the B3LYR/6-31+G(d,p) level showed that replacement of the methyl group of *p*-cresolate with a CN group and additional replacement of hydrogen atoms with Br atoms at the ortho positions shortened the C−O bond length by 0.012 and 0.017 Å, respectively (0.029 Å in total), resulting in a CO frequency upshift of 197 cm^{-1}.

The Fe^{2+}/Fe^{3+} difference spectrum of PSII in the presence of bromoxynil exhibited a characteristic positive peak at 1516 cm^{-1} (Figure 1c and Figure 2A, solid line). Since this strong peak downshifted to 1505 cm^{-1} by 11 cm^{-1} in the sample with ioxynil (Figure 2A, dotted line) without appreciable changes in other bands in the 1800−1000 cm^{-1} region (Figure 1c,d), these peaks were attributed to the CO vibrations of the phenolic herbicides. The lower frequency of the ioxynil CO is consistent with the weaker electron withdrawing ability of I than Br.

The frequency of 1516 cm^{-1} in the Fe^{2+}/Fe^{3+} spectrum is higher than the CO frequencies of bromoxynil in ethanol solutions by 30−40 cm^{-1}. This higher frequency is consistent with the assignment to the phenolate CO group engaged in a single hydrogen bond. The DFT calculations showed that when the phenolate CO group of bromoxynil has only one hydrogen bond (Figure 5, model D), its frequency is 38 cm^{-1} higher than that of the model with the CO group having two hydrogen bonds (Figure 5, model C, and Table 1), which are probably realized in ethanol. In contrast, when protonated bromoxynil accepts one hydrogen bond at the OH group oxygen (Figure 5, model B), its CO frequency is lower by 9 cm^{-1} than that of the model fully hydrogen bonded (Figure 5, model A, and Table 1). The most probable candidate for the donor of a hydrogen bond to the phenolate CO group is the imidazole NH group of the His ligand to the non-heme iron as discussed below.

Thus, the results of the CN and CO bands of bromoxynil and ioxynil in the Fe^{2+}/Fe^{3+} difference spectra strongly suggest that these phenolic herbicides are bound to the Q_B pocket as a phenolate anion form singly hydrogen bonded at the CO group.

Interaction with a His Side Chain. Fe^{2+}/Fe^{3+} difference spectra involve the vibrations of His side chains that function as ligands to the non-heme iron. The peaks at 1111(+), 1102(−), and 1094(−) cm^{-1} in the control PSII (Figure 1a) have been assigned to the CN stretching vibrations of imidazole (*36*, *38*). The negative peak at 1094 cm^{-1} has been interpreted as indicating deprotonation of one imidazole ligand in the Fe^{3+} state, probably D1-His215 in the Q_B binding site (*38*). In the presence of DCMU (Figure 1b), the 1111(+) and 1102(−) cm^{-1} peaks were virtually unchanged, whereas when bromoxynil and ioxynil were bound to PSII, these peaks slightly downshifted to 1109(+) and 1101(−) cm^{-1}, respectively, with increased relative intensities. The 1094 cm^{-1} peak almost disappeared, indicative of fully protonated D1-His215. The assignment of the 1109 and 1101 cm^{-1} peaks to the His side chain was confirmed by the 7 cm^{-1} downshifts upon global ^{15}N substitution (Figure 4A). The changes in the His CN bands may reflect the presence of a strong coupling between the non-heme iron and the phenolic herbicides that affects the vibrations of the His ligands. The most plausible view is that the phenolate CO of the phenolic herbicides interacts with the imidazole NH group of D1-His215 forming a strong hydrogen bond. It is noted that the negative band at 1094 cm^{-1} was diminished also in the presence of DCMU (Figure 1b) and disappeared in the presence of *o*-phenanthroline (*38*). Thus, the pK_a of D1-His215 in the Fe^{3+} state seems to be sensitive to the binding of herbicides in the Q_B pocket, and hence, the single negative band around 1100 cm^{-1} does not necessarily indicate the presence of a strong hydrogen bond interaction.

A positive band at 1187 cm^{-1} in the presence of bromoxynil was also sensitive to ^{15}N labeling, showing a differential signal at 1189/1178 cm^{-1} in the unlabled-minus-^{15}N-labeled double difference spectrum (Figure 4A). A similar signal was previously observed at 1179/1169 cm^{-1} in the unlabeled-minus-[^{15}N]His-labeled double difference spectrum of Q_A^-/Q_A and was assigned to the NH bending vibration of the His side chain hydrogen-bonded with Q_A (*43*). The higher frequency compared with that of 4-methylimidazole in aqueous solution at 1151 cm^{-1} was attributed to strong hydrogen bonding between Q_A and His (*43*). Since the signal similar to the 1187 cm^{-1} band was detected in the presence of ioxynil at 1185 cm^{-1} (Figure 1d) but no corresponding band was observed in the samples without herbicides and with DCMU (Figure 1a,b), this feature in the Fe^{2+}/Fe^{3+} spectrum may be specific to phenolic herbicides. Thus, the observation of the higher-frequency NH bending band supports the presence of a strong hydrogen bond at the His NH group interacting with phenolic herbicides.

The strong hydrogen bonding interaction of the His side chain in the presence of phenolic herbicides was also expressed by the presence of a broad continuum band above 2500 cm^{-1} with several Fermi resonance peaks of a His NH stretching vibration (Figure 3Ac,d, solid lines). The broad feature, which originates from a polarized proton in a strong hydrogen bond (*41*), was significantly larger in the presence of phenolic herbicides (Figure 3Ac,d, solid lines) than in the absence of herbicides (Figure 3Aa) and in the presence of other types of herbicides such as DCMU (Figure 3Ab), bromacil, atrazine (data not shown), and *o*-phenanthroline (*38*). In addition, the Fermi resonance peaks of the His NH vibration, indicative of the presence of a strongly hydrogen bonded NH group of imidazole (*42*−*46*), were intensified by phenolic herbicides (Figure 3Ac,d, solid lines).

Thus, the CN stretching, NH bending, and NH stretching vibrations, which showed the behaviors characteristic of phenolic herbicides in the Fe^{2+}/Fe^{3+} difference spectra, show that the NH group of a His ligand, most probably D1-His215, provides a strong hydrogen bond to bromoxynil and ioxynil in the Q_B pocket. This view is consistent with the conclusion that these herbicides take a phenolate anion form because of its strong basicity to enable the formation of a strong hydrogen bond.

Binding Site of Bromoxynil in the Q_B Pocket. Our docking calculation showed that bromoxynil in the phenolate anion form is bound to the Q_B pocket interacting with the imidazole NH group of D1-His215 at the CO group (Figure 6c). The CN group seems to interact with the backbone NH group of D1-Phe265. This orientation is similar to that of PQ-1; one CO group is hydrogen bonded to His215 and the other CO group to the backbone NH group of Phe265 and the OH group of Ser264 (Figure 6a). The interaction of the deprotonated bromoxynil with His215 may be much stronger than that of PQ-1 judging from the significantly shorter O···H distance of 1.63 Å for bromoxynil compared with the distance of 1.89 Å for PQ-1 (Figure 6a,b). The predicted interaction of the deprotonated bromoxynil is in agreement with the FTIR conclusion given above: the phenolic CO group of bromoxynil forms a strong hydrogen bond with the His NH group. In contrast, protonated bromoxynil was found to be oriented to the opposite side in the pocket; the phenolic OH group interacts with the backbone C=O group of D1-Ala263 and the backbone NH group of D1-Phe265 (Figure 6d). In this docking site, D1-His215 is free from interaction, and thus, the structural coupling between the non-heme iron and bromoxynil is predicted to be negligible. This is totally inconsistent with the view from FTIR spectroscopy. The docking calculation of DCMU also showed no direct interaction with D1-His215, but the C=O group of DCMU interacted with the OH group of D1-Ser264 and the backbone NH group of D1-Phe265 (Figure 6b). This is consistent with the previous observations of DCMU resistance by Ser264 mutations (*5*, *6*).

We have very recently detected the CN bands of bromoxynil in the Fe^{2+}/Fe^{3+} spectra of the PSII core complexes of *T. elongatus*, which have PsbA1 or PsbA3 as the D1 protein (*54*). Although the bands at 2200 and 2210 cm^{-1} for PSII with PsbA1 were very similar to the 2202 and 2215 cm^{-1} bands in this study using spinach PSII membranes, additional weak bands were observed at 2216 and 2232 cm^{-1} for PSII with PsbA3. The higher frequencies by ∼20 cm^{-1} of this minor signal compared with the major signal are in agreement with the higher frequency of protonated bromoxynil by 20 cm^{-1} than that of the deprotonated form in ethanol (Figure 3Be). Thus, this observation seems to indicate that a small population of bromoxynil in this PSII core complex exists as a protonated form and occupies the site as shown in Figure 6d. The observation that such a center showed a thermoluminescence temperature by $S_2Q_A^-$ recombination higher by ∼20 °C than that of the center with major CN peaks and similar to that of the PSII with DCMU (*54*) also supports the view that bromoxynil having higher-frequency CN peaks does not interact with His215 but rather interacts with the Phe265/Ser264 side.

Implication of the Interaction of Bromoxynil in the Q_B Pocket. From the FTIR spectroscopy results described above and docking calculations, we conclude that the phenolic herbicides, bromoxynil and ioxynil, are bound to the Q_B pocket in

their phenolate anion forms strongly hydrogen bonded with the NH group of D1-His215 at the CO group and most likely with the backbone NH group of D1-Phe265 at the CN group. This binding site is consistent with the previous mutagenesis data in which D1-Ser264 mutations showed no tolerance for phenolic herbicides (*4*−*6*). Taking a deprotonated form upon binding to the Q_B pocket is reasonable when taking into account the strong acidity of the phenolic OH groups of these herbicides [e.g., pK_a = 4.2 for bromoxynil (*55*)] and stabilization of the phenolate CO group by a strong hydrogen bond with D1-His215. It is noted that deprotonation of phenolic herbicides is not due to the relatively high pH (pH 8.0) used in this study, because virtually identical CN and CO bands of bromoxynil were detected in the Fe^{2+}/Fe^{3+} difference spectrum measured at pH 5.5 (data not shown).

It has been known that the redox potential of Q_A downshifts upon binding of phenolic herbicides whereas it upshifts upon DCMU binding (*11*−*13*). This redox potential downshift caused by phenolic herbicides has been considered to be responsible for accelerated photodamage by facilitating $P680^+Pheo^-$ charge recombination to produce a harmful triplet state (*11*, *12*). The mechanism of the change in the Q_A redox potential by phenolic herbicides has been attributed to the electrostatic effect by the negative charge of the phenolate form or the protein conformational changes by herbicide binding (*13*, *20*). We have previously proposed that the Q_A potential shift is caused by the change in the hydrogen bonding interaction at the CO group of Q_A (*16*) from the FTIR study in which the CO stretching vibration of Q_A^- slightly downshifted and upshifted upon binding of phenolic herbicides and other types of herbicides, respectively. The view from this study that the phenolate anions of phenolic herbicides form a stronger hydrogen bond with His215 than the hydrogen bond of PQ in the Q_B site and DCMU does not directly interact with this His is consistent with the orders of Q_A redox potentials and the Q_A^- CO frequencies. Thus, this correlation among the Q_A redox potential, the hydrogen bond strength of His215, and the hydrogen bond strength of the Q_A^- CO group provides strong evidence that the redox potential of Q_A is controlled by the hydrogen bond interaction at the His215 NH group, rather than the electrostatic effect of the negative charge of the phenolate anion. The change in the hydrogen bond strength at the His215 NH group is probably transferred to Q_A through the Q_A-His-Fe-His-(herbicide/Q_B) molecular bridge. Such a molecular interaction represents the versatility of a His side chain, which can be simultaneously engaged in a hydrogen bond and metal coordination at different nitrogen sites influencing each other through conjugated π electrons.

REFERENCES

1. Renger, G., and Holzwarth, A. R. (2005) Primary electron transfer. In Photosystem II: The Light-Driven Water:Plastoquinone Oxidoreductase (Wydrzynski, T., and Satoh, K., Eds.) pp 139−175, Springer, Dordrecht, The Netherlands.
2. Hillier, W., and Messinger, J. (2005) Mechanism of photosynthetic oxygen production. In Photosystem II: The Light-Driven Water: Plastoquinone Oxidoreductase (Wydrzynski, T., and Satoh, K., Eds.) pp 567−608, Springer, Dordrecht, The Netherlands.
3. Petrouleas, V., and Crofts, A. R. (2005) The quinone iron acceptor complex. In Photosystem II: The Light-Driven Water:Plastoquinone Oxidoreductase (Wydrzynski, T., and Satoh, K., Eds.) pp 177−206, Springer, Dordrecht, The Netherlands.
4. Oettmeier, W. (1999) Herbicide resistance and supersensitivity in photosystem II. *Cell. Mol. Life Sci. 55*, 1255–1277.
5. Trebst, A. (1987) The three-dimensional structure of the herbicide binding niche on the reaction center polypeptides of photosystem II. *Z. Naturforsch. C 42*, 742–750.
6. Trebst, A. (1996) The molecular basis of plant resistance to photosystem II herbicides. In Molecular genetics and evolution of pesticide resistance (Brown, T. M., Ed.) pp 44−51, ACS Symposium Series 645, American Chemical Society, Washington, DC.
7. Trebst, A. (2007) Inhibitors in the functional dissection of the photosynthetic electron transport system. *Photosynth. Res. 92*, 217–224.
8. Ferreira, K. N., Iverson, T. M., Maghlaoui, K., Barber, J., and Iwata, S. (2004) Architecture of the photosynthetic oxygen-evolving center. *Science 303*, 1831–1838.
9. Guskov, A., Kern, J., Gabdulkhakov, A., Broser, M., Zouni, A., and Saenger, W. (2009) Cyanobacterial photosystem II at 2.9-Å resolution and the role of quinones, lipids, channels and chloride. *Nat. Struct. Mol. Biol. 16*, 334–342.
10. Kawakami, K., Umena, Y., Kamiya, N., and Shen, J.-R. (2009) Location of chloride and its possible functions in oxygen-evolving photosystem II revealed by X-ray crystallography. *Proc. Natl. Acad. Sci. U.S.A. 106*, 8567–8572.
11. Rutherford, A. W., and Krieger-Liszkay, A. (2001) Herbicide-induced oxidative stress in photosystem II. *Trends Biochem. Sci. 26*, 648–653.
12. Krieger-Liszkay, A., Fufezan, C., and Trebst, A. (2008) Singlet oxygen production in photosystem II and related protection mechanism. *Photosynth. Res. 98*, 551–564.
13. Krieger-Liszkay, A., and Rutherford, A. W. (1998) Influence of herbicide binding on the redox potential of the quinone acceptor in photosystem II. Relevance to photodamage and phytotoxicity. *Biochemistry 37*, 17339–17344.
14. Vass, I., and Demeter, S. (1982) Classification of photosystem II inhibitors by thermodynamic characterization of the thermoluminescence of inhibitor-treated chloroplasts. *Biochim. Biophys. Acta 682*, 496–499.
15. Cser, K., and Vass, I. (2007) Radiative and non-radiative charge recombination pathways in Photosystem II studied by thermoluminescence and chlorophyll fluorescence in the cyanobacterium *Synechocystis* 6803. *Biochim. Biophys. Acta 1767*, 233–243.
16. Takano, A., Takahashi, R., Suzuki, H., and Noguchi, T. (2008) Herbicide effect on the hydrogen-bonding interaction of the primary quinone electron acceptor Q_A in photosystem II as studied by Fourier transform infrared spectroscopy. *Photosynth. Res. 98*, 159–167.
17. Noguchi, T., and Berthomieu, C. (2005) Molecular analysis by vibrational spectroscopy. In Photosystem II: The Light-Driven Water:Plastoquinone Oxidoreductase (Wydrzynski, T., and Satoh, K., Eds.) pp 367−387, Springer, Dordrecht, The Netherlands.
18. Noguchi, T. (2007) Light-induced FTIR difference spectroscopy as a powerful tool toward understanding the molecular mechanism of photosynthetic oxygen evolution. *Photosynth. Res. 91*, 59–69.
19. Berthomieu, C., and Hienerwadel, R. (2009) Fourier transform infrared (FTIR) spectroscopy. *Photosynth. Res. 101*, 157–170.
20. Roberts, A. G., Gregor, W., Britt, R. D., and Kramer, D. M. (2003) Acceptor and donor-side interactions of phenolic inhibitors in photosystem II. *Biochim. Biophys. Acta 1604*, 23–32.
21. Ono, T., and Inoue, Y. (1986) Effects of removal and reconstitution of the extrinsic 33, 24 and 16 kDa proteins on flash oxygen yield in photosystem II particles. *Biochim. Biophys. Acta 850*, 380–389.
22. Noguchi, T., Ono, T., and Inoue, Y. (1995) Direct detection of a carboxylate bridge between Mn and Ca^{2+} in the photosynthetic oxygen-evolving center by means of Fourier transform infrared spectroscopy. *Biochim. Biophys. Acta 1228*, 189–200.
23. Suzuki, H., Taguchi, Y., Sugiura, M., Boussac, A., and Noguchi, T. (2006) Structural perturbation of the carboxylate ligands to the manganese cluster upon Ca^{2+}/Sr^{2+} exchange in the S-state cycle of photosynthetic oxygen evolution as studied by flash-induced FTIR difference spectroscopy. *Biochemistry 45*, 13454–13464.
24. Frisch, M. J., Trucks, G. W., Schlegel, H. B., Scuseria, G. E., Robb, M. A., Cheeseman, J. R., Montgomery, J. A., Jr., Vreven, T., Kudin, K. N., Burant, J. C., Millam, J. M., Iyengar, S. S., Tomasi, J., Barone, V., Mennucci, B., Cossi, M., Scalmani, G., Rega, N., Petersson, G. A., Nakatsuji, H., Hada, M., Ehara, M., Toyota, K., Fukuda, R., Hasegawa, J., Ishida, M., Nakajima, T., Honda, Y., Kitao, O., Nakai, H., Klene, M., Li, X., Knox, J. E., Hratchian, H. P., Cross, J. B., Bakken, V., Adamo, C., Jaramillo, J., Gomperts, R., Stratmann, R. E., Yazyev, O., Austin, A. J., Cammi, R., Pomelli, C., Ochterski, J. W., Ayala, P. Y., Morokuma, K., Voth, G. A., Salvador, P., Dannenberg, J. J., Zakrzewski, V. G., Dapprich, S., Daniels, A. D., Strain, M. C., Farkas, O., Malick, D. K., Rabuck, A. D., Raghavachari, K., Foresman, J. B., Ortiz, J. V., Cui, Q., Baboul, A. G., Clifford, S., Cioslowski, J., Stefanov, B. B., Liu, G., Liashenko, A., Piskorz, P., Komaromi, I., Martin, R. L., Fox, D. J., Keith, T., Al-Laham, M. A., Peng, C. Y., Nanayakkara, A., Challacombe, M., Gill, P. M. W.,

Johnson, B., Chen, W., Wong, M. W., Gonzalez, C., and Pople, J. A. (2004) Gaussian 03, revision C.02, Gaussian, Inc., Wallingford, CT.
25. Becke, A. D. (1993) Density-functional thermochemistry. III. The role of exact exchange. *J. Chem. Phys. 98*, 5648–5652.
26. Lee, C., Yang, W., and Parr, R. G. (1988) Development of the Colle-Salvetti correlation-energy formula into a functional of the electron density. *Phys. Rev. B 37*, 785–789.
27. Word, J. M., Lovell, S. C., Richardson, J. S., and Richardson, D. C. (1999) Asparagine and glutamine: Using hydrogen atom contacts in the choice of side-chain amide orientation. *J. Mol. Biol. 285*, 1735–1747.
28. Rappé, A. K., Casewit, C. J., Colwell, K. S., Goddard, W. A., III, and Skiff, W. M. (1992) UFF, a full periodic table force field for molecular mechanics and molecular dynamics simulations. *J. Am. Chem. Soc. 114*, 10024–10035.
29. Nakano, T., Kaminuma, T., Uebayasi, M., and Nakata, Y. (2001) 3D structure based atomic charge calculation for molecular mechanics and molecular dynamics simulations. *Chem.-Biol. Inform. J. 1*, 35–40.
30. Nakano, T., Kaminuma, T., Sato, T., Akiyama, Y., Uebayasi, M., and Kitaura, K. (2000) Fragment molecular orbital method: Application to polypeptides. *Chem. Phys. Lett. 318*, 614–618.
31. BioStation, version 3.2 (2009) AdvanceSoft Corp., Tokyo.
32. Rappé, A. K., and Goddard, W. A., III (1991) Charge equilibration for molecular-dynamics simulations. *J. Phys. Chem. 95*, 3358–3363.
33. Huey, R., Morris, G. M., Olson, A. J., and Goodsell, D. S. (2007) A semi-empirical free energy force field with charge-based desolvation. *J. Comput. Chem. 28*, 1145–1152.
34. AutoDock 4.2 and AutoDockTools (2009) The Scripps Research Institute, La Jolla, CA.
35. Morris, G. M., Goodsell, D. S., Halliday, R. S., Huey, R., Hart, W. E., Belew, R. K., and Olson, A. J. (1998) Automated docking using a Lamarckian genetic algorithm and an empirical binding free energy function. *J. Comput. Chem. 19*, 1639–1662.
36. Hienerwadel, R., and Berthomieu, C. (1995) Bicarbonate binding to the non-heme iron of photosystem II investigated by FTIR difference spectroscopy and ^{13}C-labeled bicarbonate. *Biochemistry 34*, 16288–16297.
37. Noguchi, T., and Inoue, Y. (1995) Identification of FTIR signals from the non-heme iron in photosystem II. *J. Biochem. 118*, 9–12.
38. Berthomieu, C., and Hienerwadel, R. (2001) Iron coordination in photosystem II: Interaction between bicarbonate and the Q_B pocket studied by Fourier transform infrared spectroscopy. *Biochemistry 40*, 4044–4052.
39. Aoyama, C., Suzuki, H., Sugiura, M., and Noguchi, T. (2008) Flash-induced FTIR difference spectroscopy shows no evidence for structural coupling of bicarbonate to the oxygen-evolving Mn cluster in photosystem II. *Biochemistry 47*, 2760–2765.
40. Takahashi, R., Boussac, A., Sugiura, M., and Noguchi, T. (2009) Structural coupling of a tyrosine side chain with the non-heme iron center in photosystem II as revealed by light-induced Fourier transform infrared difference spectroscopy. *Biochemistry 48*, 8994–9001.
41. Zundel, G. (1988) Proton transfer in and proton polarizability of hydrogen bonds: IR and theoretical studies regarding mechanisms in biological systems. *J. Mol. Struct. 177*, 43–68.
42. Breton, J., and Nabedryk, E. (1998) Proton uptake upon quinone reduction in bacterial reaction centers: IR signature and possible participation of a highly polarizable hydrogen bond network. *Photosynth. Res. 55*, 301–307.
43. Noguchi, T., Inoue, Y., and Tang, X.-S. (1999) Hydrogen bonding interaction between the primary quinone acceptor Q_A and a histidine side chain in photosystem II as revealed by Fourier transform infrared spectroscopy. *Biochemistry 38*, 399–403.
44. Suzuki, H., Nagasaka, M., Sugiura, M., and Noguchi, T. (2005) Fourier transform infrared spectrum of the secondary quinone electron acceptor Q_B in photosystem II. *Biochemistry 44*, 11323–11328.
45. Iwata, T., Paddock, M. L., Okamura, M. Y., and Kandori, H. (2009) Identification of FTIR bands due to internal water molecules around the quinone binding sites in the reaction center from *Rhodobacter sphaeroides*. *Biochemistry 48*, 1220–1229.
46. Noguchi, T., Inoue, Y., and Tang, X.-S. (1999) Structure of a histidine ligand in the photosynthetic oxygen-evolving complex as studied by light-induced Fourier transform infrared difference spectroscopy. *Biochemistry 38*, 10187–10195.
47. Socrates, G. (1994) Infrared Characteristic Group Frequencies, pp 54−55, John Wiley & Sons, Chichester, U.K.
48. Berthomieu, C., Boussac, A., Mäntele, W., Breton, J., and Nabedryk, E. (1992) Molecular changes following oxidoreduction of cytochrome *b*559 characterized by Fourier transform infrared spectroscopy and electron paramagnetic resonance: Photooxidation in photosystem II and electrochemistry of isolated cytochrome *b*559 and iron protoporphyrin IX-bisimidazole model compounds. *Biochemistry 31*, 11460–11471.
49. Hasegawa, K., Ono, T., and Noguchi, T. (2000) Vibrational spectra and *ab initio* DFT calculations of 4-methylimidazole and its different protonation forms: Infrared and Raman markers of the protonation state of a histidine side chain. *J. Phys. Chem. B 104*, 4253–4265.
50. Fischer, G., and Wydrzynski, T. (2001) Isotope effects in FTIR difference spectra of the photosynthetic oxygen-evolving catalytic site determined by *ab initio* calculations on model compounds. *J. Phys. Chem. B 105*, 12894–12901.
51. Mackay, S. P., and O'Malley, P. J. (1993) Molecular modeling of the interaction between DCMU and the Q_B-binding site of photosystem II. *Z. Naturforsch. C 48*, 191–198.
52. Sobolev, V., and Edelman, M. (1995) Modeling the quinone-B binding-site of the photosystem-II reaction center using notions of complementarity and contact-surface between atoms. *Proteins 21*, 214–225.
53. Takahashi, R., and Noguchi, T. (2007) Criteria for determining the hydrogen bond structures of a tyrosine side chain by FTIR spectroscopy: DFT analyses of model hydrogen bonded complexes of *p*-cresol. *J. Phys. Chem. B 111*, 13833–13844.
54. Sugiura, M., Kato, Y., Takahashi, R., Suzuki, H., Watanabe, T., Noguchi, T., Rappaport, F., and Boussac, A. (2010) Energetics in photosystem II from *Thermosynechococcus elongatus* with a D1 protein encoded by either the *psbA1* or *psbA3* gene. *Biochim. Biophys. Acta* (in press).
55. Cessna, A. J., and Grover, R. (1978) Spectrophotometric determination of dissociation constants of selected acid herbicides. *J. Agric. Food Chem. 26*, 289–292.